# Candidates for the $5\alpha$ condensed state in $^{20}$Ne

S. Adachi,[1, *] Y. Fujikawa,[2] T. Kawabata,[1] H. Akimune,[3] T. Doi,[2] T. Furuno,[4] T. Harada,[2]
K. Inaba,[2] S. Ishida,[5] M. Itoh,[5] C. Iwamoto,[6] N. Kobayashi,[4] Y. Maeda,[7] Y. Matsuda,[5]
M. Murata,[4] S. Okamoto,[2] A. Sakaue,[8] R. Sekiya,[2] A. Tamii,[4] and M. Tsumura[2]

[1]*Department of Physics, Osaka University, Machikaneyama, Toyonaka, Osaka, Japan 560-0043*
[2]*Department of Physics, Kyoto University, Kitashirakawa-Oiwake, Sakyo, Kyoto 606-8502, Japan*
[3]*Department of Physics, Konan University, Higashinada, Kobe, Hyogo 658-8501, Japan*
[4]*Research Center for Nuclear Physics (RCNP), Osaka University, Ibaraki, Osaka 567-0047, Japan*
[5]*Cyclotron and Radioisotope Center (CYRIC), Tohoku University, Sendai, Miyagi 980-8578, Japan*
[6]*RIKEN Center for Advanced Photonics, RIKEN, Hirosawa, Wako, Saitama 351-0198, Japan*
[7]*Faculty of Engineering, University of Miyazaki, Gaukuen-Kibanadai, Miyazaki 889-2192, Japan*
[8]*Nishina Center for Accelerator Based Science, RIKEN, Hirosawa, Wako, Saitama 351-0198, Japan*
(Dated: May 10, 2021)

We conducted the coincidence measurement of $\alpha$ particles inelastically scattered from $^{20}$Ne at $0°$ and decay charged particles in order to search for the alpha-particle condensed state. We compared the measured excitation-energy spectrum and decay branching ratio with the statistical-decay-model calculations, and found that the newly observed states at $E_x = 23.6$, $21.8$, and $21.2$ MeV in $^{20}$Ne are strongly coupled to a candidate for the $4\alpha$ condensed state in $^{16}$O. This result presents the first strong evidence that these states are the candidates for the $5\alpha$ condensed state.

The alpha-cluster correlation between two protons and two neutrons is a very important property of atomic nuclei. Because an alpha particle consisting of four nucleons is tightly bound and has no excited state up to 20 MeV, it behaves as a well-established subunit in nuclei. It is theoretically suggested that alpha clusters might condense into the same lowest $0s$ orbit in their common mean field at low densities and temperatures due to their bosonic nature. This is the Bose-Einstein condensation in the nucleon many-body systems [1].

At lower densities than the nuclear saturation density $n_0 \approx 0.16$ fm$^{-3}$ and low temperatures, nuclear matter is no longer uniform and the system minimizes its energy by forming clusters such as deuterons, tritons, helium-3s, and alpha particles. The alpha particles, which are the most tightly bound among these clusters, are deposited in nuclear matter below a critical density and form the alpha-particle condensate.

One of the remarkable effects of the alpha-particle condensation is the enhancement of the symmetry energy of nuclear matter. The symmetry energy is conventionally defined as the quadratic coefficient when the internal energy per nucleon of nuclear matter is expanded as the Taylor series of the asymmetry parameter $\delta = (n_n - n_p)/n_B$. Here, $n_n$, $n_p$, and $n_B$ denote the number densities of neutrons, protons, and baryons, respectively. The density and temperature dependence of the symmetry energy is of great importance to describe nuclear matter. If the formation of clusters in nuclear matter is taken into account, the internal energies per nucleon are considerably lowered around $\delta = 0$, particularly at low temperatures. Therefore, the symmetry energy, which is the curvature of the internal energy with respect to $\delta$, substantially increases at low densities below $n_B \sim 10^{-2}$ fm$^{-3}$ [2–4]. The equation of state (EoS) of

nuclear matter is hence influenced by the alpha-particle condensation. Construction of the EoS is one of the ultimate goals in nuclear physics not only because it is the benchmark of our understanding about strongly interacting fermions but also because it is required to describe many astrophysical phenomena such as neutron stars, supernovae, and the nucleosynthesis in the universe.

The alpha-particle condensation is expected to manifest as the alpha-particle condensed states (ACSs) in finite nuclei as well as in nuclear matter. We can study dilute nuclear matter by examining the ACSs even though infinite nuclei can not be formed on the earth. The properties of the ACSs such as energies and widths will shed light on low-density nuclear matter.

The authors of Refs. [1, 5] proposed the Tohsaki-Horiuchi-Schuck-Röpke (THSR) wave function to describe the $0^+$ states in $^8$Be, $^{12}$C, and $^{16}$O, and theoretically suggested the ACSs emerge near the $2\alpha$, $3\alpha$, and $4\alpha$-decay threshold energies, respectively. The THSR wave function demonstrates that these states are low-density states composed of weakly interacting alpha particles condensed into the lowest $0s$ orbit, and are akin to the alpha-particle condensate in nuclear matter. The following work [6] predicted that similar ACSs should exist slightly above $k\alpha$-decay thresholds in heavier self-conjugate $A = 4k$ nuclei up to $k \sim 10$. In order to establish the alpha-particle condensation as a dilute phase of nuclear matter, it should be examined whether the ACSs universally exist in heavier nuclei. However, the experimental information on the ACSs was obtained in limited nuclei so far.

Let us briefly describe the present situation on the ACSs in the self-conjugate $A = 4k$ nuclei. The ground state of $^8$Be and the $0_2^+$ state in $^{12}$C locate near the $2\alpha$ and $3\alpha$-decay thresholds, and are nicely described with

the spatially developed wave functions by the fully microscopic alpha-cluster models [5, 7, 8] and the Green's function Monte Carlo calculation [9]. These wave functions reasonably well reproduce the energies and inelastic form factors of these states and are almost equivalent to the THSR wave functions for the $2\alpha$ and $3\alpha$ condensed states [5, 10]. These facts are strong evidence that the ground state of $^8$Be and the $0_2^+$ state in $^{12}$C are the ACSs. The exotic structures of these ACSs highly motivate further theoretical studies with various models such as the antisymmetrized molecular dynamics method [11], the fermionic molecular dynamics method [12], the chiral effective field theory [13], and the algebraic cluster model [14, 15]. The ACSs are discussed also in non-self-conjugate nuclei, e.g. in Refs. [16, 17].

The ACS in $^{16}$O was theoretically predicted to be the $0_6^+$ state with the width of 140 keV [18–20]. The excited state at $E_x = 15.097 \pm 0.005$ MeV with the width of $166 \pm 30$ keV [21] is proposed to be the corresponding state. Although this state was observed in many reactions [21], it was pointed out in Ref. [22] that this state might be contaminated with a previously unidentified resonance which does not exhibit $0^+$ character. Recently it was found that this state decays into the $^8$Be$(0_1^+) + {}^8$Be$(0_1^+)$ or $^{12}$C$(0_2^+) + \alpha$ channel with the almost same probabilities [23]. The $0_6^+$ state in $^{16}$O is, therefore, a strong candidate of the ACS.

For $^{20}$Ne and heavier nuclei, no known states are assigned to the ACSs. Only a tentative candidate for the $5\alpha$ condensed state was experimentally proposed. The several $0^+$ states observed in the $^{22}$Ne$(p, t)^{20}$Ne reaction were examined with the shell-model calculation [24]. It was found that one of the $0^+$ states at $E_x = 22.5$ MeV was not described by the shell model, and its excitation energy is close to $E_x = 21.14$ MeV where the $5\alpha$ condensed state is predicted in Ref. [6]. However, the excitation energy is not conclusive evidence for the ACS because many $0^+$ states exist around the expected excitation energy. Further information is necessary to identify the ACS. It should be noted that the decay property of the excited state provides additional information. Because all the alpha particles in the ACSs occupy the same lowest $0s$ orbit, the wave functions of the alpha particles in the ACSs of different nuclei are similar and the overlap between them should be large. Therefore, ACSs should prefer to decay via ACSs in lighter nuclei by emitting alpha particles. Because energy differences between ACSs are smaller than a few MeV [6], emission of low-energy $\alpha$ particles from $0^+$ states near $k\alpha$-decay thresholds can be a clue to identify ACSs.

The ACS might be dynamically accessed via heavy-ion collision and fusion reaction [25, 26]. It is worthy to mention the recent measurement of the $^{12}$C$(^{16}$O$, {}^{28}$Si$^*$) reaction [27]. Decay alpha particles were comprehensively detected to obtain the invariant-mass spectra of $^{16}$O, $^{20}$Ne, and $^{24}$Mg, but no ACSs were found. The au-

thors claimed that the Coulomb barrier inherently suppresses low-energy-particle decays and obscures the signature of the ACSs. However, some of the authors previously pointed out that the Coulomb barrier in the ACSs should be suppressed due to their dilute nature [28]. One plausible explanation for this contradictory situation is that the ACSs were hidden by a lot of backgrounds from various high-spin states in Ref. [27] because large angular momenta were brought to the system in the heavy-ion collision. Since ACSs have the spin and parity of $0^+$ and isospin of 0, nuclear reactions which selectively excite isoscalar $0^+$ states should be employed to populate ACSs. One of the best reactions to populate isoscalar $0^+$ states is inelastic alpha scattering at forward angles [29]. Because both the spin and isospin of the alpha particle are 0, the inelastic alpha scattering off self-conjugate $A = 4k$ nuclei selectively excites isoscalar natural-parity states. In addition, the cross sections for the $0^+$ states have their maximum at $0°$.

In the present work, we carried out the coincidence measurement of alpha particles inelastically scattered from $^{20}$Ne at $0°$ and decay charged particles emitted from excited states in order to search for the $5\alpha$ condensed state in $^{20}$Ne.

The experiment was conducted at the Research Center for Nuclear Physics (RCNP), Osaka University. The experimental setup was almost the same with Ref. [30] except for a $^{20}$Ne gas target and a Si telescope array.

A 386-MeV $^4$He$^{2+}$ beam with an intensity of about 10 nA was transported to an isotopically enriched $^{20}$Ne gas target. The $^{20}$Ne gas with the enrichment of 99.95% was filled in the target cell at 14.1 kPa and room temperature. The thickness of the target cell along the beam axis was 8.0 mm, which corresponds to the mass thickness of 89.6 $\mu$g/cm$^2$ of the $^{20}$Ne gas. The entrance and exit windows of the target cell were sealed with 100 nm-thick silicon nitride (SiN$_x$) membranes. The square membranes with the size of 10 mm × 10 mm were glued on the target cell.

Alpha particles inelastically scattered from the target were analyzed using the magnetic spectrometer Grand Raiden [31]. The backgrounds from the SiN$_x$ membranes were subtracted by using the measurement with the empty cell. We found that oil mists from vacuum pumps deposited on the SiN$_x$ membrane and caused $^{nat}$C background. The $^{nat}$C background was successfully subtracted by using the measurement with $^{nat}$C foil. Figure 1 shows the excitation-energy spectra for the $^{20}$Ne gas target, the empty cell with $^{nat}$C, and the $^{nat}$C foil.

In order to detect decay particles, we installed a Si telescope array around the target covering 0.42 sr (3.4% of $4\pi$) at $\theta_{\mathrm{lab}} = 106.4$–$163.0°$. The Si telescope array consisted of six segments, which were placed 170 mm away from the target. Each segment had three layers of Si detectors, but only the first and second layers were used in the present analysis. The thicknesses of the first and second layers were 65 $\mu$m and 500 $\mu$m respectively,
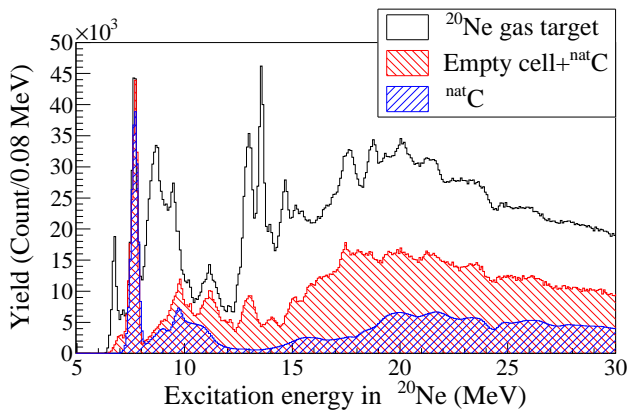
FIG. 1. Excitation-energy spectra for the $^{20}$Ne gas target (black open), the empty cell with $^{nat}$C (red hatched), and $^{nat}$C foil (blue hatched). The spectra of the empty cell with $^{nat}$C and the $^{nat}$C foil are scaled for the subtraction.

in order from the target side, and their dimensions were 50 mm × 50 mm. The first layers were divided into 8 strips and the second layers were read as a single pad. The first Si detectors had a dead layer with a thickness of about 1.2 $\mu$m on the rear side. The detection threshold of decay particles was 0.53 MeV.

Particle identification (PID) for decay particles that penetrated the first layer was performed by using the correlation between the energy loss in the first layer and the total energy ($\Delta E$–$E$ method). This $\Delta E$–$E$ method succeeded in separating decay alpha particles from hydrogen isotopes with an accuracy of almost 100%, and the $\Delta E$–$E$ method could be applied to reject protons at higher particle energies than 2.45 MeV. On the other hand, the time of flight from the target to the Si detector and the total energy were used for low-energy particles which stopped at the first layer (TOF method). The time of flight was obtained from the time difference between the radio-frequency signals from the cyclotron and the timing signals of the Si detectors. As the kinetic energy of decay particles decreased, the resolution of the time of flight got worse. Therefore, it was required to narrow the gate width for the time of flight to prevent the contamination due to hydrogen isotopes. The PID accuracy and efficiency were determined as a function of the particle energy by analyzing the time-of-fight spectra at different energies. Typically, for the decay particles with the kinetic energy of 1 MeV, the PID efficiency for alpha particles was 69% and the 12% of detected hydrogen isotopes was misidentified as alpha particles.

Figure 2 shows the correlation between the kinetic energies of decay alpha particles ($K_\alpha$) and the excitation energies of $^{20}$Ne [$E_x(^{20}$Ne)]. Linear loci corresponding to the $\alpha$-decay events into the ground, $0_2^+$, and $2_1^+$ states in $^{16}$O are clearly seen. In the two-body decay of $^{20}$Ne into the $^{16}$O + $\alpha$ channel, $K_\alpha$ correlates with $E_x(^{20}$Ne)
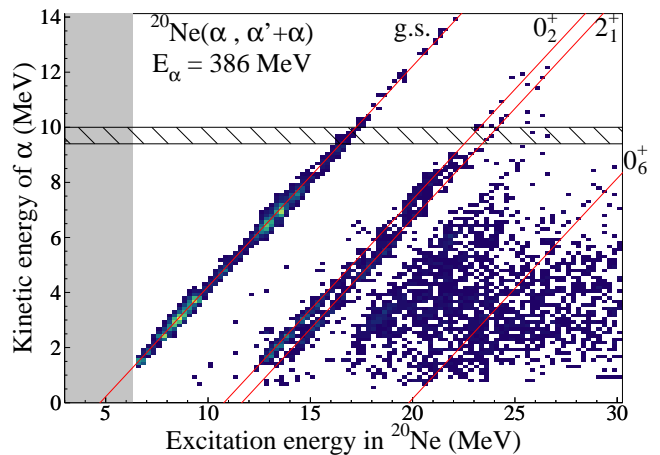


FIG. 2. Correlation between the kinetic energy of decay alpha particles ($K_\alpha$) and the excitation energies of $^{20}$Ne. The red solid lines indicate the calculated correlation in the $\alpha$-decay events into the ground, $0_2^+$, $2_1^+$, and $0_6^+$ states in $^{16}$O. The alpha particles with $K_\alpha < 9.7$ MeV stopped at the first layer of the Si detectors. $K_\alpha$ in the hatched area are accompanied by uncertainties due to the dead layer of the Si detectors. The shaded area represents the excitation-energy region out of the momentum acceptance of the Grand Raiden spectrometer.

via the excitation energy of $^{16}$O [$E_x(^{16}$O)] as

$$K_\alpha = \frac{m_{^{16}O}}{m_{^{16}O} + m_\alpha} \left[ E_x(^{20}\text{Ne}) - E_{th}(^{16}\text{O} + \alpha) - E_x(^{16}\text{O}) \right].$$

$E_{th}(^{16}$O + $\alpha$) is the threshold energy for the $^{16}$O + $\alpha$ decay in $^{20}$Ne, and $m_{^{16}O(\alpha)}$ is the rest mass of $^{16}$O (the $\alpha$ particle).

Figure 3(a) shows the excitation-energy spectrum of the $^{20}$Ne($\alpha, \alpha'$) reaction at 0° for the singles events obtained by measuring inelastically scattered alpha particles only. No clear peaks are observed around a few MeV above the 5$\alpha$ decay threshold where the ACS is expected. Figure 3(b) shows the excitation-energy spectrum for the coincidence events in which one alpha particle was detected by the Si telescope array. The obtained yield was corrected with the PID efficiency for alpha particle, and converted to the cross section on the basis of the fact that the $\alpha$-decay probability of the $0_2^+$ state at $E_x = 6.73$ MeV in $^{20}$Ne is almost 100% [32] The error bars of the spectrum in Fig. 3(b) are calculated by quadratically adding the statistical errors and the systematic errors in the PID analysis. Note that the cross sections for the $^{20}$Ne($\alpha, \alpha' + \alpha$) reaction in Fig. 3(b) can be apparently larger than those for the $^{20}$Ne($\alpha, \alpha'$) reaction in Fig. 3(a) above the $^{12}$C + 2$\alpha$ threshold because more than one alpha particle is allowed to be emitted. It is remarkable that the two narrow peaks are observed at $E_x = 23.6$ and 21.8 MeV above the 5$\alpha$ decay threshold, where no peaks are seen in Fig. 3(a) although their statistical significance is not large.
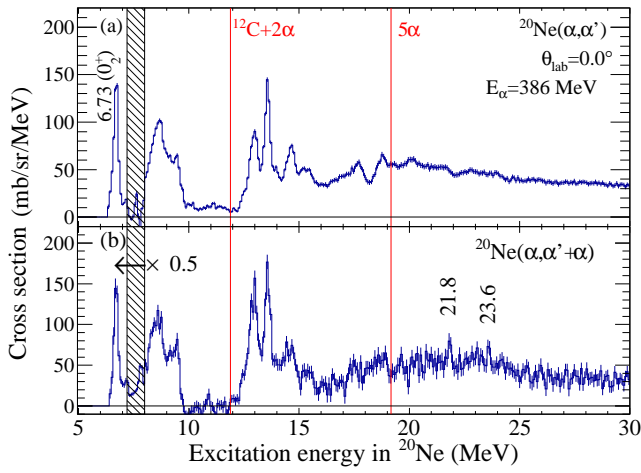
FIG. 3. Excitation-energy spectra of the $^{20}$Ne$(\alpha, \alpha')$ reaction at 0° for (a) the singles events and (b) the coincidence events. The error bars in the lower panel include the systematic errors in the PID analysis as well as the statistical errors. The spectra at $E_x < 8.0$ MeV are downscaled by a factor of 0.5. The hatched area indicates the excitation-energy region where a strong peak due to the $0_2^+$ state in the $^{12}$C contaminants caused large errors in the background subtraction. The vertical lines at $E_x = 11.9$ and 19.2 MeV represent the $^{12}$C $+ 2\alpha$ and $5\alpha$ decay thresholds.



FIG. 4. Excitation-energy spectra same as Fig. 3(b) but when $E_x(^{16}$O$)$ is (a) $14.1 \pm 0.5$ MeV, (b) $15.1 \pm 0.5$ MeV, and (c) $16.1 \pm 0.5$ MeV. The statistical-decay-model calculations for the $0^+$ and $2^+$ states in $^{20}$Ne are shown together with thin red solid and green dashed lines. The vertical lines at 21.2, 21.8, and 23.6 MeV are drawn to guide the eyes. The dead layers of the Si detectors caused the uncertainty on the kinetic energies of alpha particles in the hatched area as for Fig. 2.

In order to search for the $5\alpha$ condensed state, we focused on the $\alpha$-decay events into the $0_6^+$ state in $^{16}$O because this state is a strong candidate for the $4\alpha$ condensed state. We reconstructed $E_x(^{16}$O$)$ from $K_\alpha$ and $E_x(^{20}$Ne$)$ assuming the two-body $^{20}$Ne$^* \rightarrow {}^{16}$O$+\alpha$ decay and selected the events with $E_x(^{16}$O$) = 15.1 \pm 0.5$ MeV to obtain the excitation-energy spectrum of $^{20}$Ne in the $^{20}$Ne$(\alpha, \alpha' + \alpha)^{16}$O$(0_6^+)$ reaction as shown in Fig. 4(b). The same normalization factor with Fig. 3(b) was used to convert the yield to the cross section. The similar spectra for the events in the 1.0-MeV lower and higher $E_x(^{16}$O$)$ ranges were also shown in Figs. 4(a) and (c) for comparison. The error bars in Fig. 4 include the statistical errors and the systematic errors in the PID analysis as in Fig. 3(b). For example, the cross section at $E_x(^{20}$Ne$) = 21.2$ MeV in Fig. 4(b) is $7.9 \pm 1.3$ (stat.) $\pm 0.8$ (sys.) $= 7.9 \pm 1.5$ mb/sr/MeV/1 MeV.

The excitation-energy spectra in Fig. 4 were compared with the theoretical spectra calculated by the statistical-decay model. This model takes into account the spins, parities, isospins, energies, and level densities of the mother and its descendant nuclei as well as transmission coefficients for decay particles. Decay branching ratios of excited states in $^{20}$Ne into particle- ($\alpha$, $p$, and $n$) and $\gamma$-decay channels were calculated with the computer code CASCADE [33] assuming that the initial excited state is the isoscalar state with its spin and parity of $0^+$, $1^-$, or $2^+$. Using the theoretical branching ratios, we performed
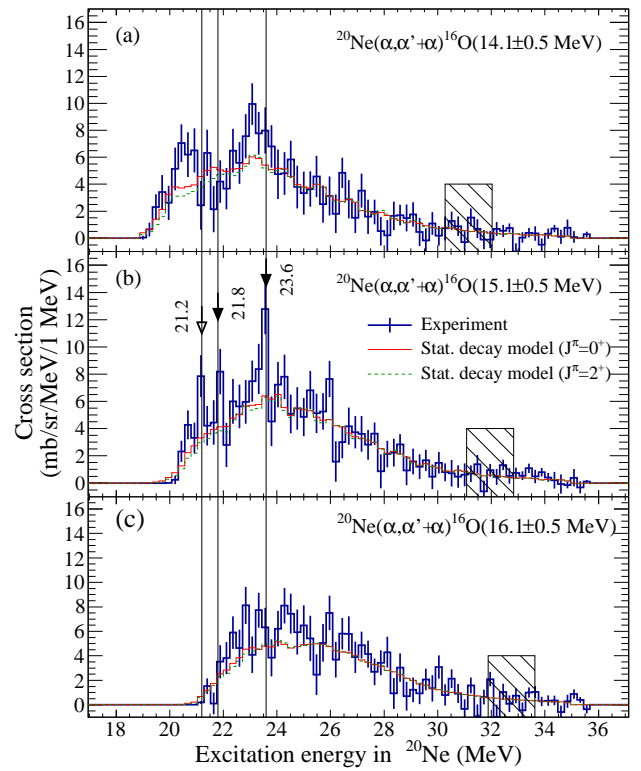
the Monte Carlo calculation to simulate the decay processes of the excited states in $^{20}$Ne. The decay processes were traced until all of the descendant nuclei settled in their ground states under the assumption that decay particles were emitted isotropically in the rest frame of the decaying nuclei. The simulated decay events were analyzed in the same manner with the experimental data after the energies of decay particles were randomly varied according to the experimental resolution of 0.40 MeV at the full width at half maximum. The theoretical spectra for the $0^+$, $1^-$, and $2^+$ states were almost the same, and the cross section for the $1^-$ state in the inelastic alpha scattering is generally smaller than those for the $0^+$ and $2^+$ states at 0°. Therefore, only the theoretical spectra for the $0^+$ and $2^+$ states are presented in Fig. 4. The theoretical spectra in Figs. 4(a), (b), and (c) were multiplied by a factor of 0.74. This factor is determined in Fig. 4(b) to fit the theoretical spectrum for the $0^+$ state to the experimental spectrum at $E_x = 27$–31 MeV where no structures were observed in the experimental spectrum. In contrast to the good agreement between the theoreti-
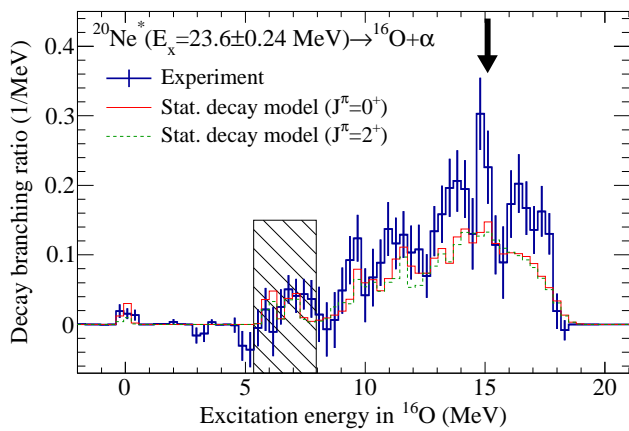
FIG. 5. Decay branching ratio of the excited state in $^{20}$Ne at $E_x = 23.6 \pm 0.24$ MeV populated by the inelastic alpha scattering at $0°$ (thick blue solid lines with error bars) compared with the statistical-decay-model calculations from the isoscalar $0^+$ and $2^+$ states in $^{20}$Ne (thin red solid and green dashed lines). The dead layers of the Si detectors caused the uncertainty on the kinetic energies of alpha particles in the hatched area as for Fig. 2.

cal calculations and the experiment above $E_x = 26$ MeV in Fig. 4, the two peaks at $E_x = 23.6$ and 21.8 MeV, which were observed in Fig. 3(b), were visible in Fig. 4(b) as indicated by the solid arrows but not in Figs. 4(a) and (c). It demonstrates that these two states strongly couple to the $0_6^+$ state in $^{16}$O. The experimental cross section in Fig. 4(b) also exceeds the calculations at $E_x = 21.2$ MeV as indicated by the open arrow, where no clear peak structures are seen in Fig. 3(b). This peak is not observed in Figs. 4(b) and (c). The 21.2-MeV state is closer to the $5\alpha$ threshold than the two states at $E_x = 23.6$ and 21.8 MeV. The similar excess is also observed in $E_x = 24$–26 MeV although the statistical uncertainty is large.

In order to examine the decay properties of the new state at $E_x = 23.6$ MeV in $^{20}$Ne, the $\alpha$-decay events at $E_x = 23.6 \pm 0.24$ MeV were selected, and the decay branching ratio into $^{16}$O was obtained assuming the two-body decay as shown in Fig. 5. The theoretical branching ratios of the isoscalar $0^+$ and $2^+$ states at the same excitation energy ($E_x = 23.6 \pm 0.24\,\text{MeV}$) were obtained from the simulated decay events using the same normalization factor as in Fig. 4, and compared with the experiment. The theoretical branching ratios do not change much depending on the spins of the initial excited states. Several prominent peaks were observed on the continuous spectrum calculated by the statistical-decay model. It should be noted that the location of the strongest peak around $E_x(^{16}\text{O}) = 15$ MeV agrees with that of the $0_6^+$ state in $^{16}$O at $E_x(^{16}\text{O}) = 15.1$ MeV indicated by the vertical arrow.

Figures 4 and 5 show that the newly found excited state at $E_x = 23.6$ MeV is strongly coupled to the $0_6^+$

state in $^{16}$O, which is a candidate for the $4\alpha$ condensed state. This 23.6-MeV state is a candidate for the $5\alpha$ condensed state. However, the measured excitation energy is considerably higher than the theoretical value of $E_x = 21.14$ MeV [6]. This might suggest another interpretation that either of the low-energy states at $E_x = 21.8$ or 21.2 MeV corresponds to the $5\alpha$ condensed state, and the 23.6-MeV state is akin to the $5\alpha$ condensed state like the $2_2^+$ state in $^{12}$C, which is an excited state of the relative motion of alpha clusters in the $3\alpha$ condensed state [7, 8, 34, 35].

The high-lying structures around $E_x = 24$–26 MeV in Fig. 4(b) might be analogous to the $0^+$ states above the $4\alpha$ condensed state in $^{16}$O, which are coupled to the $\alpha + {}^{12}\text{C}(0_2^+)$ channel as predicted in Ref. [36]. In another interpretation, these structures might be due to the fragmentation of alpha-cluster states which is discussed in medium-mass nuclei [37, 38].

In order to clarify the correspondence between these new states and the $5\alpha$ condensed state, it is necessary to determine their spins and parities. Regrettably, the spins and parities of the new states could not be assigned in the present work. However, it is worthy to mention that the states at 21.2 and 21.8 MeV are very close to the tentative $0^+$ states at 21.16 and 21.80 MeV reported in Ref. [24]. This fact also supports their candidacy for the $5\alpha$ condensed state.

In summary, we conducted the coincidence measurement of alpha particles inelastically scattered from $^{20}$Ne at $0°$ and decay charged particles from excited states in order to search for the $5\alpha$ condensed state in $^{20}$Ne. Comparing the measured excitation-energy spectra and decay branching ratio with the statistical-decay-model calculation, we found that the newly observed states at $E_x = 23.6$, 21.8, and 21.2 MeV in $^{20}$Ne are strongly coupled to the $0_6^+$ state in $^{16}$O. This result presents the first strong evidence that these states are the candidates for the $5\alpha$ condensed state in $^{20}$Ne because the $0_6^+$ state in $^{16}$O is a strong candidate for the $4\alpha$ condensed state. However, their spins and parities are still ambiguous. An additional measurement to determine their spins and parities is strongly desired.

* adachi@ne.phys.sci.osaka-u.ac.jp

[1] A. Tohsaki, H. Horiuchi, P. Schuck, and G. Röpke, Physical Review Letters 87, 192501 (2001).

[2] S. Typel, G. Röpke, T. Klähn, D. Blaschke, and H. H. Wolter, Physical Review C 81, 015803 (2010).

[3] S. Typel, H. H. Wolter, G. Röpke, and D. Blaschke, European Physical Jounal A **50**, 17 (2014).

[4] Z. W. Zhang and L. W. Chen, Physical Review C **100**, 054304 (2019).

[5] Y. Funaki, H. Horiuchi, A. Tohsaki, P. Schuck, and G. Röpke, Progress of Theoretical Physics **108**, 297 (2002).

[6] T. Yamada and P. Schuck, Physical Review C **69**, 024309 (2004).

[7] M. Kamimura, Nuclear Physics A **351**, 456 (1981).

[8] E. Uegaki, Y. Abe, S. Okabe, and H. Tanaka, Progress of Theoretical Physics **57**, 1262 (1979).

[9] R. B. Wiringa, S. C. Pieper, J. Carlson, and V. R. Pandharipande, Physical Review C **62**, 014001 (2000).

[10] Y. Funaki, A. Tohsaki, H. Horiuchi, P. Schuck, and G. Röpke, Physical Review C **67**, 051306(R) (2003).

[11] Y. Kanada-En'yo, M. Kimura, and A. Ono, Progress of Theoretical and Experimental Physics **2012**, 01A202 (2012).

[12] M. Chernykh, H. Feldmeier, T. Neff, P. von Neumann-Cosel, and A. Richter, Physical Review Letters **98**, 032501 (2007).

[13] E. Epelbaum, H. Krebs, T. A. Lähde, D. Lee, and U.-G. Meißner, Physical Review Letters **109**, 252501 (2012).

[14] D. J. Marín-Lámbarri, R. Bijker, M. Freer, M. Gai, Tz. Kokalova, D. J. Parker, and C. Wheldon, Physical Review Letters **113**, 012502 (2014).

[15] R. Bijker and F. Iachello, Progress in Particle and Nuclear Physics **110**, 103735 (2020).

[16] T. Yamada and Y. Funaki, Physical Review C **92**, 034326 (2015).

[17] K. Inaba, T. Kawabata, Y. Sasamoto, M. Fujiwara, K. Hatanaka, K. Itoh, M. Itoh, K. Kawase, H. Matsubara, Y. Maeda, K. Nakanishi, K. Suda, S. Sakaguchi, Y. Shimizu, A. Tamii, Y. Tameshige, M. Uchida, T. Uesaka, and H. P. Yoshida, in *JPS Conference Proceedings*, Vol. 31 (2020) p. 011069.

[18] Y. Funaki, T. Yamada, H. Horiuchi, G. Röpke, P. Schuck, and A. Tohsaki, Physical Review Letters **101**, 082502 (2008).

[19] T. Yamada, Y. Funaki, T. Myo, H. Horiuchi, K. Ikeda, G. Röpke, P. Schuck, and A. Tohsaki, Physical Review C **85**, 034315 (2012).

[20] Y. Funaki, Physical Review C **97**, 021304(R) (2018).

[21] D. R. Tilley, H. R. Weller, and C. M. Chevesyc, Nuclear Physics A **565**, 1 (1993).

[22] K. C. Li, R. Neveling, P. Adsley, P. Papka, F. D. Smit, J. W. Brümmer, C. A. Diget, M. Freer, M. N. Harakeh, T. Kokalova, F. Nemulodi, L. Pellegri, B. Rebeiro, J. A. Swartz, S. Triambak, J. J. van Zyl, and C. Wheldon, Physical Review C **95**, 031302(R) (2017).

[23] M. Barbui, K. Hagel, J. Gauthier, S. Wuenschel, R. Wada, V. Z. Goldberg, R. T. deSouza, S. Hudan, D. Fang, X. G. Cao, and J. B. Natowitz, Physical Review C **98**, 044601 (2018).

[24] J. A. Swartz, B. A. Brown, P. Papka, F. D. Smit, R. Neveling, E. Z. Buthelezi, S. V. Förtsch, M. Freer, Tz. Kokalova, J. P. Mira, F. Nemulodi, J. N. Orce, W. A. Richter, and G. F. Steyn, Physical Review C **91**, 034317 (2015).

[25] J. Vadas, T. K. Steinbach, J. Schmidt, V. Singh, C. Haycraft, S. Hudan, R. T. deSouza, L. T. Baby, S. A. Kuvin, and I. Wiedenhöver, Physical Review C **92**, 064610 (2015).

[26] B. Schuetrumpf and W. Nazarewicz, Physical Review C **96**, 064608 (2017).

[27] J. Bishop, Tz. Kokalova, M. Freer, L. Acosta, M. Assié, S. Bailey, G. Cardella, N. Curtis, E. DeFilippo, D. DellAquila, S. DeLuca, L. Francalanza, B. Gnoffo, G. Lanzalone, I. Lombardo, N. S. Martorana, S. Norella, A. Pagano, E. V. Pagano, M. Papa, S. Pirrone, G. Politi, F. Rizzo, P. Russotto, L. Quattrocchi, R. Smith, I. Stefan, A. Trifirò, M. Trimarchì, G. Verde, M. Vigilante, and C. Wheldon, Physical Review C **100**, 034320 (2019).

[28] Tz. Kokalova, N. Itagaki, W. von Oertzen, and C. Wheldon, Physical Review Letters **96**, 192502 (2006).

[29] M. N. Harakeh and A. v. d. Woude, *Giant Resonance: Fundamental High-Frequency Modes of Nuclear Excitation* (Oxford University Press, 2001).

[30] M. Itoh, H. Sakaguchi, M. Uchida, T. Ishikawa, T. Kawabata, T. Murakami, H. Takeda, T. Taki, S. Terashima, N. Tsukahara, Y. Yasuda, M. Yosoi, U. Garg, M. Hedden, B. Kharraja, M. Koss, B. K. Nayak, S. Zhu, H. Fujimura, M. Fujiwara, K. Hara, H. P. Yoshida, H. Akimune, M. N. Harakeh, and M. Volkerts, Physical Review C **68**, 064602 (2003).

[31] M. Fujiwara, H. Akimune, I. Daito, H. Fujimura, Y. Fujita, K. Hatanaka, H. Ikegami, I. Katayama, K. Nagayama, N. Matsuoka, S. Morinobu, T. Noro, M. Yoshimura, H. Sakaguchi, Y. Sakemi, A. Tamii, and M. Yosoi, Nuclear Instruments and Methods in Physics Research, Section A: A

[32] D. R. Tilley, C. M. Cheves, J. H. Kelley, S. Raman, and H. R. Weller, Nuclear Physics A **636**, 249 (1998).

[33] F. Pühlhofer, Nucluear Physics A **280**, 267 (1977).

[34] P. Descouvemont and D. Baye, Physical Review C **36**, 54 (1987).

[35] Y. Funaki, Physical Review C **92**, 021302(R) (2015).

[36] Y. Funaki, T. Yamada, H. Horiuchi, G. Röpke, P. Schuck, and A. Tohsaki, Progress of Theoretical Physics Supplement **196**, 439 (2012).

[37] M. Norrby, *Alpha-Cluster Structures in Medium Light Nuclei*, Ph.D. thesis, Åbo Akademi University (2011).

[38] S. Bailey, T. Kokalova, M. Freer, C. Wheldon, R. Smith, J. Walshe, N. Curtis, N. Soić, L. Prepolec, V. Tokić, F. M. Marqués, L. Achouri, F. Delaunay, Q. Deshayes, M. Parlog, B. Fernández-Dominguez, B. Jacquot, and A. Soylu, Physical Review C **100**, 051302(R) (2019).

[39] A. K. Nurmukhanbetova, V. Z. Goldberg, D. K. Nauruzbayev, M. S. Golovkov, and A. Volya, Physical Review C **100**, 062802(R) (2019).

[40] M. Itoh, H. Akimune, M. Fujiwara, U. Garg, H. Hashimoto, T. Kawabata, K. Kawase, S. Kishi, T. Murakami, K. Nakanishi, Y. Nakatsugawa, B. K. Nayak, H. Sakaguchi, S. Terashima, M. Uchida, Y. Yasuda, M. Yosoi, and J. Zenihiro, Journal of Physics: Conference Series **569**, 012009 (2014).